REGULAR PAPER

Investigation of high speed β-Ga_2O_3 growth by solid-source trihalide vapor phase epitaxy

Japanese Journal of Applied Physics **62**, SF1021 (2023) **REGULAR PAPER**
https://doi.org/**10.35848/1347-4065/acc747**

Investigation of high speed β-Ga_2O_3 growth by solid-source trihalide vapor phase epitaxy

Kyohei Nitta[1], Kohei Sasaki[2], Akito Kuramata[2], and Hisashi Murakami[1*]

[1]*Department of Applied Chemistry, Tokyo University of Agriculture and Technology, 2-24-16 Naka-cho, Koganei, Tokyo 184-8588, Japan*
[2]*Novel Crystal Technology Inc., 2-3-1 Sayama, Saitama 350-1328, Japan*

*E-mail: murak@cc.tuat.ac.jp

Received December 14, 2022; revised February 27, 2023; accepted March 23, 2023; published online April 14, 2023

Trihalide vapor phase epitaxy (THVPE) is a new type of halide vapor phase epitaxy (HVPE) that uses $GaCl_3$ as a group III source, enabling Ga_2O_3 growth without particle generation, although the growth rate is low. In this study, β-Ga_2O_3 is grown by THVPE using solid $GaCl_3$ as a group III precursor. The growth rate increases linearly with increasing partial pressure of the precursor. The dependence of the growth rate on the VI/III ratio is revealed on sapphire substrates, with the growth rate reaching a maximum at a VI/III ratio of 95. We have also obtained a growth rate of 32.2 μm h^{-1} on β-Ga_2O_3 (001) substrates with no particle generation, crystal quality equivalent to that of the substrate, and high purity equivalent to that of HVPE.

1. Introduction

Gallium oxide (Ga_2O_3) has many polymorphs: α, β, γ, δ and ε phases.[1,2] Each phase has a crystalline structure and semiconducting properties with different band gaps.[3–8] Among them, the β-phase is the most stable one and has a monoclinic structure with a large band gap of ~4.5 eV,[9,10] which is wider than those of semiconductor materials, such as SiC (3.3 eV)[11] and GaN (3.4 eV),[12] and high breakdown electric field.[13] Therefore, β-Ga_2O_3 is a prospective material for low-loss and high-voltage power devices. Several power devices, such as Schottky barrier diodes[14–16] and MOS field-effect transistors, have recently been demonstrated.[17–19] Furthermore, β-Ga_2O_3 can be produced via melt growth, which is difficult to achieve in SiC or GaN without high temperature and pressure.[20–27] β-Ga_2O_3 bulk single crystals are grown using melting methods, such as Czochralski,[20,21] vertical Bridgman,[22] floating zone,[23] and edge-defined film-fed growth (EFG),[24,25] to produce large-diameter substrates.[25] Alternatively, thin film epitaxial growth of β-Ga_2O_3 has been actively studied using MBE,[28–30] pulsed laser deposition,[31] metal organic CVD (MOCVD),[32,33] and halide vapor phase epitaxy (HVPE).[34–37]

High-speed homoepitaxial growth with high purity has been successfully achieved via HVPE using gallium monochloride (GaCl) as a group-III precursor.[34] Homoepitaxial growth of a thick β-Ga_2O_3 layer on a 2 inch diameter (001) substrate has also been demonstrated via HVPE.[35] Moreover, one of the presenting authors has demonstrated that the n-type carrier density can be precisely controlled in a wide range of 10^{15}–10^{19} cm^{-3} by changing the amount of Si dopant.[36] However, the HVPE of Ga_2O_3 has a large equilibrium constant for Ga_2O_3 formation, i.e. a substantial change occurs in the free energy of the formation reaction.[37] Generally, the larger the free energy change of the formation reaction, the smaller the nucleation radius. Hence, the HVPE of β-Ga_2O_3 tends to generate particles before reaching the substrate surface owing to the gas phase reaction in the reactor, which can degrade the crystalline quality of the growth layer. Additionally, particles become the origin for abnormal growth, which hinders long-term growth. On the other hand, trihalide vapor phase epitaxy (THVPE), which uses gallium trichloride ($GaCl_3$) as a group III precursor, has a relatively small free energy change for Ga_2O_3 formation,[37] therefore, it is expected to inhibit the formation of Ga_2O_3 particles in the reactor. Although β-Ga_2O_3 growth via THVPE was demonstrated without particle formation,[38] the maximum β-Ga_2O_3 growth rate for THVPE was limited to ~6 μm h^{-1}, which is smaller than that for HVPE; the growth rate for HVPE was demonstrated to be up to 20 μm h^{-1} without the degradation of crystal quality.[37] Furthermore, in a previous study on β-Ga_2O_3 growth via THVPE, $GaCl_3$ was generated through a two-step reaction in the source zone (directly connected to the reaction zone) as follows:[38]

$$Ga(l) + 1/2\ Cl_2(g) \rightleftarrows GaCl(g) \quad (1)$$

$$GaCl(g) + Cl_2(g) \rightleftarrows GaCl_3(g). \quad (2)$$

Therefore, it was difficult to confirm the complete conversion from GaCl to $GaCl_3$ [Eq. (2)] and precisely control the input pressure of the precursor. Moreover, because the aforementioned reactions require high temperatures, the structure of the HVPE reactor is considerably complicated, as it comprises a source and growth zones. In contrast, it was reported that THVPE uses solid $GaCl_3$ as a group-III source in GaN growth.[39] Using a $GaCl_3$ solid source as a group-III precursor in THVPE, it is easy to control its input partial pressure by changing the equilibrium vapor pressure (by specifically changing heating temperature and carrier flow rate); moreover, the equipment structure can be simplified.

In this study, the heteroepitaxial growth of β-Ga_2O_3 on sapphire substrates was conducted via solid-source THVPE. The dependence of β-Ga_2O_3 growth on the input partial pressure of $GaCl_3$ and the ratio of the O_2 input partial pressure against the input partial pressure of $GaCl_3$ (VI/III) was investigated. Additionally, high-speed homoepitaxial growth of β-Ga_2O_3 was demonstrated.

2. Experimental methods

This study used an atmospheric-pressure cold-wall growth system with a vertical quartz glass reactor for Ga_2O_3 growth. In this system, solid $GaCl_3$ with a purity of 99.9999% (Yamanaka Hutech Corporation) was used as a group III source. The solid $GaCl_3$ was encapsulated in a separate stainless container maintained at 85 °C and then sublimated. The $GaCl_3$ gas was transported to the growth reactor using a

purified N_2 carrier gas (dew point < -110 °C) and reacted with O_2 gas supplied through another line. The substrate was placed on the SiC-coated carbon susceptor, which was fixed at the center of the reactor. The substrate used for heteroepitaxial growth was sapphire (0001) without an offcut, and the growth temperature was constant at 1100 °C. The dependence of the Ga_2O_3 growth rate on the input partial pressure of $GaCl_3$ (P^0_{III}) was demonstrated for heteroepitaxial growth at a fixed VI/III ratio, where the input partial pressures of $GaCl_3$ (P^0_{III}) and O_2 (P^0_{VI}) varied in the ranges of 3.00×10^{-4}–6.00×10^{-3} atm and 1.20×10^{-2}–2.40×10^{-1} atm, respectively. The relation of the Ga_2O_3 growth rate with the VI/III ratio was also demonstrated for heteroepitaxial growth, where P^0_{III} was fixed and P^0_{VI} varied in the range of 2.14×10^{-1}–2.75×10^{-1} atm. The substrate used in homoepitaxial growth was tin-doped β-Ga_2O_3 (001) (prepared using the EFG method), and the growth temperature was set at 1150 °C. The dependence of the Ga_2O_3 growth rate on P^0_{III} was demonstrated for homoepitaxial growth, where P^0_{VI} was fixed and P^0_{III} varied in the range of 7.37×10^{-4}–4.42×10^{-3} atm.

The growth rate of the heteroepitaxial β-Ga_2O_3 layers grown on the sapphire (0001) substrates was evaluated via cross-sectional scanning electron microscopy observation. The surface morphology was observed via Nomarski differential interference contrast (NDIC) imaging. The crystal structure and quality of grown Ga_2O_3 were characterized using high-resolution X-ray diffraction, XRD pole-figure measurement, and X-ray rocking curves (XRCs). The impurity concentrations in the grown β-Ga_2O_3 layers were evaluated via secondary ion mass spectrometry (SIMS).

3. Results and discussion

3.1. Dependence of the Ga_2O_3 growth rate on input partial pressure of $GaCl_3$ and VI/III ratio in THVPE

Figure 1 shows the dependence of the Ga_2O_3 growth rate on the sapphire (0001) substrate as a function of P^0_{III}. The growth rate of Ga_2O_3 linearly increased with increasing P^0_{III} at a fixed VI/III ratio, indicating that the THVPE growth of Ga_2O_3 at >1100 °C is limited by mass transport of precursors, as predicted by the thermodynamic analysis.[37] This suggests that the growth rate can be considerably increased by increasing the supply input partial pressure of precursors.

Figure 2 shows the dependence of the Ga_2O_3 growth rate on the sapphire (0001) substrate as a function of the VI/III ratio. In the region where the VI/III ratio was <95, the growth rate of Ga_2O_3 increased with increasing VI/III ratio.

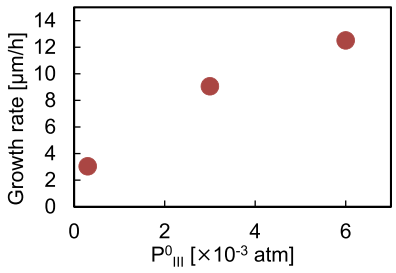

Fig. 1. Dependence of the growth rate of Ga_2O_3 on the sapphire (0001) substrate as a function of input partial pressure of the group-III precursor ($GaCl_3$) at a fixed VI/III ratio (VI/III = 80).

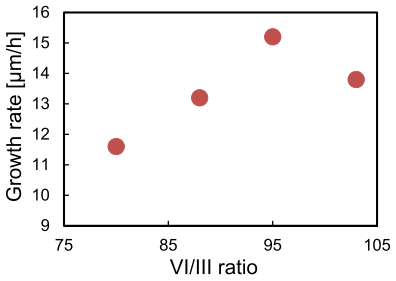

Fig. 2. Dependence of the growth rate of Ga_2O_3 on the sapphire (0001) substrate as a function of the VI/III ratio at fixed P^0_{III} ($P^0_{III} = 5.34 \times 10^{-3}$ atm).

These results agree well with the relation between the VI/III ratio and the driving force of Ga_2O_3 formation predicted by the thermodynamic analysis in a previous study.[37] However, in the region where the VI/III ratio was >95, the growth rate of Ga_2O_3 decreased with increasing VI/III ratio, which was inconsistent with the aforementioned thermodynamic analysis. This result indicates that the $GaCl_3$ source gas was consumed in the gas phase to generate fine Ga_2O_3 particles before reaching the substrate surface with increasing input partial pressure of oxygen. Therefore, while decreasing the pressure in the reactor to prevent the consumption of $GaCl_3$ in the gas phase, it might be essential to increase the growth rate by increasing the flow velocity of supplied gases while decreasing the pressure in the reactor, which is often adopted in MOCVD of AlN.[40]

3.2. High-speed homoepitaxial growth by THVPE

Figure 3 shows the dependence of the Ga_2O_3 growth rate on the β-Ga_2O_3 (001) substrate as a function of P^0_{III}. The growth rate of Ga_2O_3 increased as P^0_{III} increased, and the maximum growth rate of 32.2 μm h^{-1} was obtained at $P^0_{III} = 4.42 \times 10^{-3}$ atm. The reason for the higher growth rate on Ga_2O_3 compared to sapphire substrates may be due to the nucleation behavior caused by the difference in wettability at the crystal surface.[41] The well response of the growth rate to the P^0_{III} indicated that the input partial pressure could be easily controlled using a solid $GaCl_3$ source. Figure 4 shows an NDIC microscopy surface image of the homoepitaxial β-Ga_2O_3 layer with a growth rate of 32.2 μm h^{-1}. As can be seen from the image, the surface morphology typically observed in the case of HVPE[34,38] was observed. Additionally, particles were not observed on the surface; therefore, high-speed homoepitaxial growth of β-Ga_2O_3 without particle generation was achieved via THVPE. Furthermore, the crystalline quality of the homoepitaxial

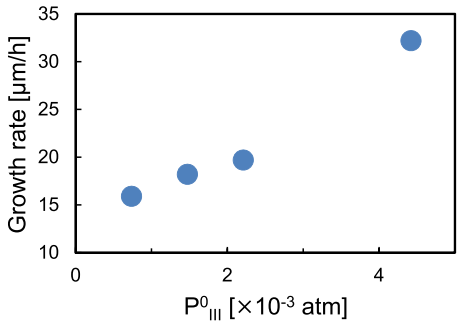

Fig. 3. Dependence of the growth rate of Ga_2O_3 on the β-Ga_2O_3 substrate as a function of P^0_{III} at fixed P^0_{VI} ($P^0_{VI} = 2.10 \times 10^{-1}$ atm).

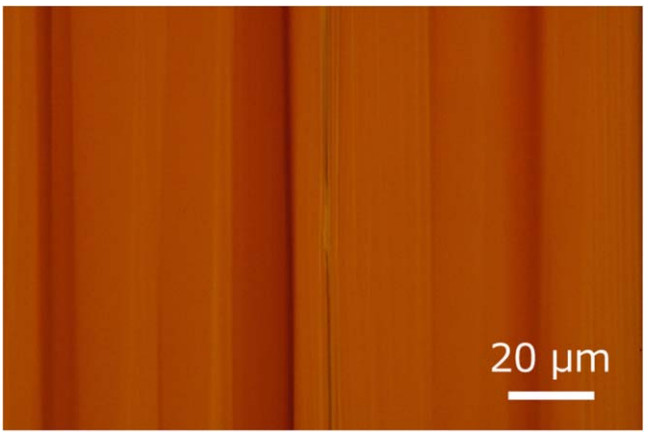

Fig. 4. Nomarski differential interference contrast (NDIC) microscopy surface images after homoepitaxial growth on the β-Ga_2O_3 (001) substrate at a growth rate of 32.2 μm h^{-1}.

β-Ga_2O_3 layer with a growth rate of 32.2 μm h^{-1} was investigated via X-ray diffraction. It was confirmed that the grown layer was a single beta phase from the XRD 2θ–ω profile (not shown); only {001}-related peaks of β-Ga_2O_3 were observed. Figure 5 shows the XRC profiles of the homoepitaxial β-Ga_2O_3 layer and β-Ga_2O_3 substrate for comparison at near the (002) symmetrical reflection and (400) skew-symmetrical reflection. The FWHM values of XRC for the sample and substrate are 50 and 55 arcsec at near (002), respectively, and 27 and 22 arcsec at near (400), respectively. Because the β-Ga_2O_3 substrate in this study was produced in the early stages of development, its quality was slightly lower than that of the currently commercialized substrate. However, because the FWHM values of the sample are almost the same as those of the β-Ga_2O_3 substrate, we speculate that the homoepitaxial layer with higher crystalline quality can be obtained on the latest substrate. According to the (−401) XRD, pole-figure measurements were also demonstrated as a comparison with the β-Ga_2O_3 substrate (not shown). It was revealed that newly introduced twins were not observed in THVPE-grown β-Ga_2O_3 because the same peaks were obtained from the substrate and sample.

Table I summarizes the impurity concentration (measured via SIMS) of the homoepitaxial layer grown via solid-source THVPE. Only nitrogen and chlorine atoms were detected in the grown crystal. Although nitrogen impurity was not detected in the β-Ga_2O_3 layer grown at 1000 °C in a previous study,[38] it was detected in the β-Ga_2O_3 layer grown via solid-source THVPE at 1150 °C. This was caused by the activation of nitrogen induction via growth at a temperature higher than that used in a previous study.[38] The carrier gas is estimated to be the origin of nitrogen; therefore, it is necessary to take measures, such as changing the carrier gas to an inert gas such as argon. Moreover, $GaCl_3$ is estimated to be the origin of chlorine. The chlorine concentration was 5×10^{16} cm^{-3}, which was slightly higher than that of HVPE-grown crystal (1×10^{16} cm^{-3})[34] and conventional THVPE-grown crystal (3×10^{16} cm^{-3}).[38] This was due to the stoichiometric increase of chlorine atoms in the group-III source from GaCl to $GaCl_3$ and a higher growth temperature than those used in previous studies. However, the chlorine concentration of the 10^{16} order was considerably low and would not affect the carrier concentration; hence, the reduction of impurity concentration is considered but not a major issue.[34] Therefore, it was confirmed that solid-source THVPE could produce high-purity homoepitaxial β-Ga_2O_3 at a high growth rate.

Table I. Impurity concentrations (measured via secondary ion mass spectrometry (SIMS)) of the homoepitaxial sample grown via solid-source trihalide vapor phase epitaxy (THVPE). (B.G.) means background level in the measurement.

Elements	C	N	Si	Cl
Impurity concentration (cm^{-3})	$<2 \times 10^{16}$ (B.G.)	5×10^{16}	$<6 \times 10^{15}$ (B.G.)	5×10^{16}

4. Conclusions

The dependence of the growth rate of Ga_2O_3 on the input partial pressure of the group-III source and VI/III ratio is demonstrated via solid-source THVPE on the sapphire (0001) and β-Ga_2O_3 (001) substrates. The growth rate linearly increases with increasing input partial pressure of the group-III source. Furthermore, the growth rate increases with the VI/III ratio, as predicted from the thermodynamic analysis, till the ratio equals to 95. The maximum growth rate (~32 μm h^{-1}) is obtained on the β-Ga_2O_3 (001) substrate, which is comparable to that in the case of HVPE, without particle formation and with high crystal quality and purity. This result suggests that the solid-source THVPE method has

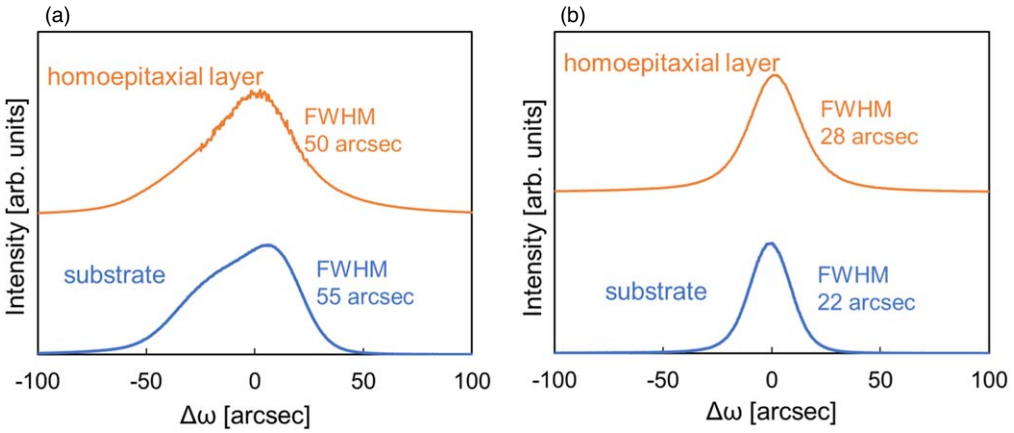

Fig. 5. X-ray rocking curve (XRC) profiles at near (a) (002) symmetrical reflection and (b) (400) skew-symmetrical reflection of the homoepitaxial β-Ga_2O_3 sample with a growth rate of 32.2 μm h^{-1} via trihalide vapor phase epitaxy (THVPE) and β-Ga_2O_3 (001) substrate.

high potential for growing the drift layer in Ga_2O_3-based power devices.

1) R. Roy, V. G. Hill, and E. F. Osborn, J. Am. Chem. Soc. **74**, 719 (1952).
2) S. Yoshioka, H. Hayashi, A. Kuwabara, F. Oba, K. Matsunaga, and I. Tanaka, J. Phys.: Condens. Matter. **19**, 346211 (2007).
3) D. Shinohara and S. Fujita, Jpn. J. Appl. Phys. **47**, 7311 (2008).
4) H. H. Tippins, Phys. Rev. **140**, A316 (1965).
5) H. Hayashi, R. Huang, H. Ikeno, F. Oba, S. Yoshioka, and I. Tanaka, Appl. Phys. Lett. **89**, 181903 (2006).
6) T. Oshima, T. Nakazono, A. Mukai, and A. Ohtomo, J. Cryst. Growth **359**, 60 (2012).
7) X. Xia, Y. Chen, Q. Feng, H. Liang, P. Tao, M. Xu, and G. Du, Appl. Phys. Lett. **108**, 202103 (2016).
8) Y. Oshima, E. G. Villora, Y. Matsushita, S. Yamamoto, and K. Shimamura, J. Appl. Phys. **118**, 085301 (2015).
9) S. Geller, J. Chem. Phys. **33**, 676 (1960).
10) T. Onuma, S. Saito, K. Sasaki, T. Masui, T. Yamaguchi, T. Honda, and M. Higashiwaki, Jpn. J. Appl. Phys. **54**, 112601 (2015).
11) J. B. Casady and R. W. Johnson, Solid State Electron. **39**, 1409 (1996).
12) I. Vurgaftman and J. R. Meyer, J. Appl. Phys. **94**, 3675 (2003).
13) M. Higashiwaki, K. Sasaki, A. Kuramata, T. Masui, and S. Yamakoshi, Appl. Phys. Lett. **100**, 013504 (2012).
14) K. Sasaki, M. Higashiwaki, A. Kuramata, T. Masui, and S. Yamakoshi, IEEE Electron Device Lett. **34**, 493 (2013).
15) C.-H. Lin et al., IEEE Electron Device Lett. **40**, 1487 (2019).
16) W. Li, K. Nomoto, Z. Hu, D. Jena, and H. G. Xing, IEEE Trans. Electron Devices **68**, 2420 (2021).
17) M. H. Wong, K. Sasaki, A. Kuramata, S. Yamakoshi, and M. Higashiwaki, IEEE Electron Device Lett. **37**, 212 (2016).
18) T. Kamimura, Y. Nakata, M. H. Wong, and M. Higashiwaki, IEEE Electron Device Lett. **40**, 1064 (2019).
19) Y. Lv et al., IEEE Electron Device Lett. **41**, 537 (2020).
20) Y. Tomm, P. Reiche, D. Klimm, and T. Fukuda, J. Cryst. Growth **220**, 510 (2000).
21) Z. Galazka et al., J. Cryst. Growth **404**, 184 (2014).
22) K. Hoshikawa, E. Ohba, T. Kobayashi, J. Yanagisawa, C. Miyagawa, and Y. Nakamura, J. Cryst. Growth **447**, 36 (2016).
23) E. G. Villora, K. Shimamura, Y. Yoshikawa, K. Aoki, and N. Ichinose, J. Cryst. Growth **270**, 420 (2004).
24) H. Aida, K. Nishiguchi, H. Takeda, N. Aota, K. Sunakata, and Y. Yaguchi, Jpn. J. Appl. Phys. **47**, 8506 (2008).
25) A. Kuramata, K. Konishi, S. Watanabe, Y. Yamaoka, T. Masui, and S. Yamakoshi, Jpn. J. Appl. Phys. **55**, 1202A2 (2016).
26) W. Utsumi, H. Saitoh, H. Kaneko, T. Watanuki, K. Aoki, and O. Shimomura, Nat. Mater. **2**, 735 (2003).
27) D. H. Hofmann and M. H. Müller, Mater. Sci. Eng. B **61–62**, 29 (1999).
28) T. Oshima, N. Arai, N. Suzuki, S. Ohira, and S. Fujita, Thin Solid Films **516**, 5768 (2008).
29) K. Sasaki, A. Kuramata, T. Masui, E. G. Villora, K. Shimamura, and S. Yamakoshi, Appl. Phys. Express **5**, 035502 (2012).
30) N. K. Kalarickal, Z. Xia, J. McGlone, S. Krishnamoorthy, W. Moore, M. Brenner, A. R. Arehart, S. A. Ringel, and S. Rajan, Appl. Phys. Lett. **115**, 152106 (2019).
31) F. B. Zhang, K. Saito, T. Tanaka, M. Nishio, and Q. X. Guo, J. Cryst. Growth **387**, 96 (2014).
32) F. Alema, B. Hertog, A. Osinsky, P. Mukhopadhyay, M. Toporkov, and W. V. Schoenfeld, J. Cryst. Growth **475**, 77 (2017).
33) G. Seryogin, F. Alema, N. Valente, H. Fu, E. Steinbrunner, A. T. Neal, S. Mou, A. Fine, and A. Osinsky, Appl. Phys. Lett. **117**, 262101 (2020).
34) H. Murakami et al., Appl. Phys. Express **8**, 015503 (2015).
35) Q. T. Thieu, D. Wakimoto, Y. Koishikawa, K. Sasaki, K. Goto, K. Konishi, H. Murakami, A. Kuramata, Y. Kumagai, and S. Yamakoshi, Jpn. J. Appl. Phys. **56**, 110310 (2017).
36) K. Goto, K. Konishi, H. Murakami, Y. Kumagai, B. Monemar, M. Higashiwaki, A. Kuramata, and S. Yamakoshi, Thin Solid Films **666**, 182 (2018).
37) K. Nomura, K. Goto, R. Togashi, H. Murakami, Y. Kumagai, A. Kuramata, S. Yamakoshi, and A. Koukistu, J. Cryst. Growth **405**, 19 (2014).
38) K. Ema, K. Sasaki, A. Kuramata, and H. Murakami, J. Cryst. Growth **564**, 126129 (2021).
39) N. Takekawa, M. Takahashi, M. Kobayashi, I. Kanosue, H. Uno, K. Takemoto, and H. Murakami, Jpn. J. Appl. Phys. **58**, SC1022 (2019).
40) A. Ubukata, Y. Yano, Y. Yamaoka, Y. Kitamura, T. Tabuchi, and K. Matsumoto, Phys. Status Solidi C **10**, 1353 (2013).
41) M. Boćkowski, I. Grzegory, S. Krukowski, B. Łucznik, M. Wróblewski, G. Kamler, J. Borysiuk, P. Kwiatkowski, K. Jasik, and S. Porowski, J. Cryst. Growth **270**, 409 (2004).